THE JOURNAL OF PHYSICAL CHEMISTRY C
A JOURNAL OF THE AMERICAN CHEMICAL SOCIETY

pubs.acs.org/JPCC

Article

High-Quality In Situ X-ray Absorption Spectroscopy Monitoring of the Palladium Nucleation inside the 3D Printed Microfluidic Chip

Arina V. Dobrovolskaya, Sergei V. Chapek, Oleg A. Usoltsev, Evgeny Naranov, Dmitry N. Gorbunov, Alexander L. Trigub, Anton L. Maximov, Alexander V. Soldatov, and Aram L. Bugaev*

Cite This: https://doi.org/10.1021/acs.jpcc.3c03266

Read Online

ACCESS | Metrics & More | Article Recommendations

ABSTRACT: An efficient approach for high-quality X-ray absorption spectroscopy (XAS) measurements is proposed and exemplified by monitoring the nucleation of palladium nanoparticles from Pd(II) acetate. The idea of an X-ray beam passing through a microfluidic channel allowed for a significant improvement of the data quality to monitor in situ the early stages of palladium nanoparticle formation. The time evolution of Pd(II) and Pd(0) fractions was followed by collecting the spectra in seven subsequent channels and quantified by linear combination analysis of Pd foil and Pd acetate reference spectra. This work illustrates the application of XAS in microfluidics for chemical systems and might be used for obtaining structural information under reaction conditions in the presence of 4*d* metals.

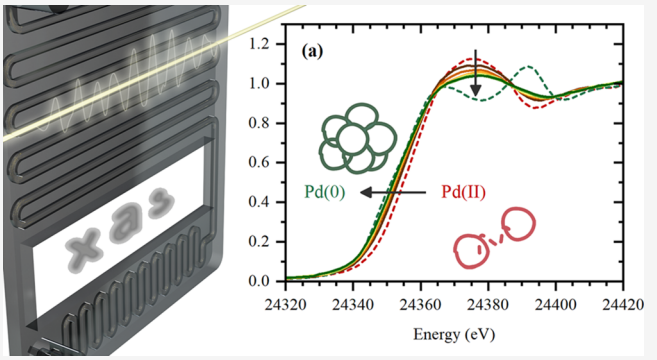

Downloaded via SOUTHERN FEDERAL UNIV on October 9, 2023 at 10:30:44 (UTC).
See https://pubs.acs.org/sharingguidelines for options on how to legitimately share published articles.

INTRODUCTION

Microfluidic technologies[1−4] are expanding into various fields, from biomedicine to inorganic chemistry. A microfluidic chip that handles a small amount of fluid (from nano to microliters) inside the channels with dimensions from tens of micrometers to millimeters can be connected to numerous online characterization tools which open new possibilities for researchers for optimization of the reaction conditions and monitoring different reaction steps with a high temporal resolution by accruing the data from spatially separated channels. The microchip materials vary from silicon with glass to polymers with glass. The use of polymers allows the application of 3D printing for fast and cheap production of the microchips.

Analysis of the processes inside the microchip in real time allows one for fast optimization of the process parameters in a fast and economical way.[5] For example, one can achieve the desired size, shape, and composition of the colloidal nanoparticles by varying the synthesis parameters. Analytical tools applied for online monitoring of the processes inside or directly after the microchip range from laboratory-based ones, such as optical microscopy, UV−vis spectroscopy,[6] Raman spectroscopy,[7] and those involving the large-scale facilities, such as synchrotron-based small-angle X-ray scattering (SAXS),[8−10] X-ray diffraction (XRD),[11] or X-ray absorption spectroscopy (XAS).[12,13] The choice of the technique strongly depends on the type of materials. For example, for gold nanoparticles, exhibiting characteristic plasmon resonance, UV−vis spectroscopy is a powerful tool, while for palladium nanoparticles, it becomes less informative, making the use of X-ray-based techniques more crucial.

There are a few examples of using microfluidic systems coupled with XAS, which were aimed at achieving the time evolution of the systems under investigation via space-resolved measurements. A group of Grunwaldt monitored the formation of gold nanoparticles[14] by progressive decrease of the white line in Au L_3-edge X-ray absorption near-edge structure (XANES) spectra, indicative of the reduction process. Variation of iron oxidation state during the reaction of iron(II) chloride with NaOH was monitored by Fe *K*-edge XANES at the SOLEIL synchrotron.[12] The early steps in the formation of CdSe nanocrystals were monitored at Se *K*-edge.[15] A group from Paul Scherrer Institute and ETH Zurich studied the calcium carbonate precipitation in a droplet-based microfluidic system by Ca *K*-edge XAS.[16] Due to microscales of the chips, the XAS quality drops with decreasing the optical pathway of the X-ray beam through the sample, which forced the usage of fluorescence mode (in contrast to transmission mode) in the above examples. Therefore, one has to spend significant time

Received: May 17, 2023
Revised: August 24, 2023

© XXXX American Chemical Society

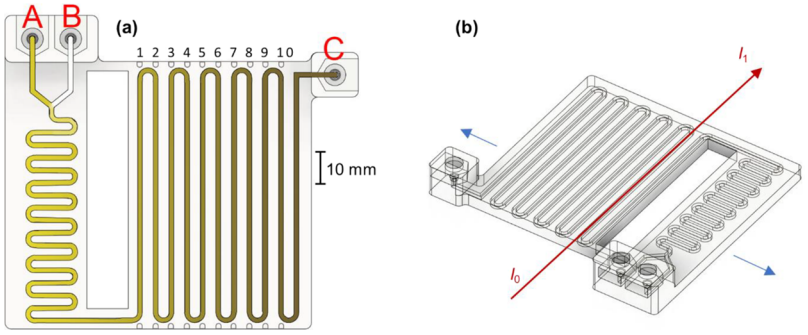

Figure 1. (a) Top view of the microchip and (b) isometric view with the direction of the beam in channel #2 (red arrow) detected by ionization chambers before (I_0) and after (I_1) the chip, and the direction of chip movement during the measurement (blue arrows).

to get extended X-ray absorption fine structure (EXAFS) data of sufficient quality or limit the data analysis by the XANES region. The advantage of high X-ray energies, such as for Pd *K*-edge, is the higher flexibility in designing the cells and sample environment for in situ measurements due to high penetration depths of X-ray photons. In particular, the cells for high pressures and temperatures were suggested.[17−19]

Here, we have developed a system based on a chip with millimeter-sized channels for the synthesis of palladium nanoparticles with in situ control by synchrotron-based XAS. The key feature of the system is the collection of high-quality XAS data in transmission geometry by aligning the microchannels with the X-ray beam. The device was successfully tested by monitoring the reduction of Pd(II) acetate to Pd(0), with the formation of small palladium nanoclusters.

MATERIALS AND METHODS

Chip Manufacturing and Characterization. The chip was designed using Fusion 360 (Autodesk, Mill Valley, CA, USA) with a total outer length of 112 mm, a depth of 100 mm, and a height of 5.5 mm. The chip (see Figure 1) consisted of two different zones: mixing and reaction zones, two inlets (A and B) and one outlet (C). The total volume of the mixing zone was 0.75 mL. The reaction zone consisted of 10 straight regions of the microchannel (referred to as channel #1, channel #2, etc.) with the length of 80 mm and the cross-section of 1.5 × 1.5 mm^2. To reduce the absorption of the X-ray beam by the walls, small cylindrical recesses (shown in Figure 1a) were made from the outer sides of the walls in the direction of the channels. For the temperature control, two silicone rubber heaters were attached to the reaction zone from the top and bottom sides and covered by 3 M thermal insulation (3 M, Saint Paul, MN, USA). The designed chip was exported into a standard tessellation language (.stl) digital file. This file was imported into Ultimaker Cura 4.13.1 (Ultimaker B.V., Utrecht, The Netherlands). The .stl file was sliced to g-code file format for fused deposition modeling (FDM) printing with 100 μm layer height and 350 μm wall line width. Both mixing and reaction zones were printed as a single piece. The Ultimaker 3D printer, which relies on fused filament fabrication (FFF) technology, was used to 3D print the microfluidic device with PETG filament (REC3D, Moscow, Russia). This filament was extruded through a stainless-steel nozzle with a diameter of 400 μm onto a glass printing platform heated to 60 °C. The manufacturing parameters are listed in Table 1.

Synthesis Procedure. Pd(II) acetate (Sigma Aldrich) was used as the palladium precursor. 20 mg of Pd acetate was dissolved in 10 mL of toluene (LenReactive) and loaded into one of the syringes (Channel A). A solution of 132 μL of triethylamine (LenReactive) was added to 10 mL of toluene and loaded in the second syringe (Channel B). The reagents were then dosed to the inlets A and B of the chip by the commercial Beyond BYZ-810 syringe pumps. The connection was done via PTFE tubes connected by HPLC fitting to the chip and Luer-lock connection to the syringes. The flow rates for channels A and B were set to 3 and 1 mL/h, respectively. The reaction zone of the chip was preheated to 50 °C and kept at this temperature during the synthetic procedure.

Table 1. Settings Used for 3D Printing of the Microfluidic Device

layer height, μm	extrusion width, μm	print temperature, °C	infill line width, μm	wall line count	top surface skin layers	infill density, %
100	350	245	420	5	4	50

X-ray Absorption Spectroscopy. Pd *K*-edge XAS data were collected at Structural Materials Science (STM) beamline of the Kurchatov synchrotron source (Moscow, Russia). The energy was selected by Si(220) channel-cut monochromator operated in the step mode. The monochromator was de-tuned to reduce the contribution of higher harmonics. The estimated photon flux was 10^7 photons/s/mm^2. The spectra were collected in the 24.1−25.2 eV range ($k_{max} \sim 15$ Å^{-1}), with a step of 10 eV in the pre-edge and 1 eV in the XANES region. In the EXAFS region, a constant step in the *k*-space of 0.05 Å^{-1} was chosen. The time per one spectrum was ca. 10 min. Pd(II) acetate was measured simultaneously with the sample using a third ionization chamber for energy calibration. Pd(0) foil was measured as the reference sample. The beam profile was ca. 0.7 × 0.7 mm^2, monitored by an X-ray camera. The long channels of the microchip were oriented parallel to the beam and aligned so that the beam could path through the central part of the microchannel without hitting its edges. The total absorption calculation and edge jump estimation were performed using Henke tables for X-ray absorption attenuation length. In particular, 80 mm of toluene resulted in a total absorption of 0.66, the absorption of both front and back walls is ca. 0.02, and the Pd(II) acetate was expected to have a total absorption of 0.5 with the edge jump of 0.42, which was in agreement with the experimentally observed one. A motorized sample stage was controlled remotely to probe the sample in different microchannels during the synthesis. All XAS data were processed and analyzed in Demeter software.[20]

https://doi.org/10.1021/acs.jpcc.3c03266
J. Phys. Chem. C XXXX, XXX, XXX−XXX

RESULTS

Application of in situ analytical tools is crucial to designing novel materials with desired properties: e.g., metal nanoparticles with controlled size, shape, and composition. X-ray absorption spectroscopy is an efficient technique that provides the oxidation state of the element of interest, coordination numbers, and interatomic distances. However, for a low-concentrated system, the amount of the element of interest (e.g., palladium) is insufficient for high-quality data collection in transmission mode. Below, we describe the setup and approach for efficient in situ control of the growth of Pd nanoparticles by XAS. The microfluidic device was installed at the automated sample stage with the microchannels oriented parallel to the X-ray beam (see Figure 2). Transmission of the X-rays along the whole length of the microchannel allowed for the optimization of the edge jump in XAS data by increasing the optical path.

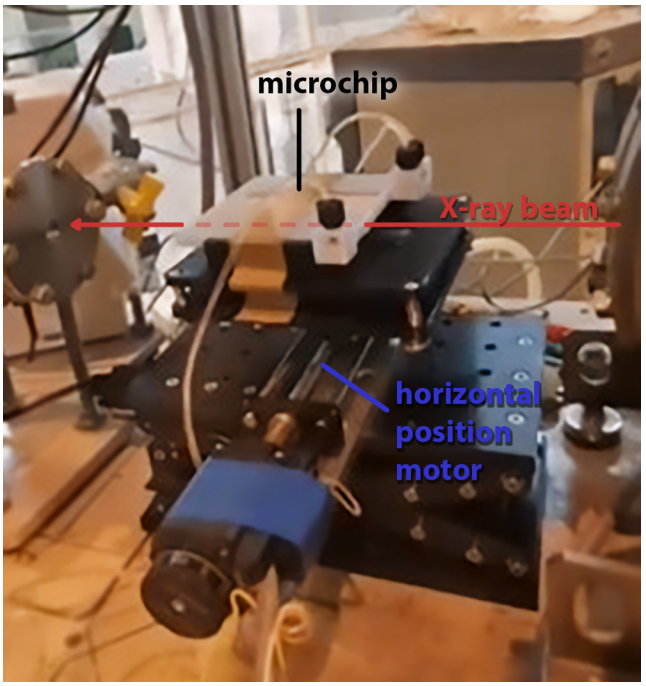

Figure 2. Photograph of the microchip installed on the automated sample stage at STM beamline.

The optimized length of the microchannels allowed for high-quality data collection in both XANES and EXAFS regions (see Figure 3). The data were collected in seven consecutive channels, each representing a specific stage in the process of palladium nanoparticle formation. In XANES data (Figure 3a), a clear transition from Pd(II) toward Pd(0) was observed, which indicated the reduction of the palladium acetate precursor. At the same time, the FT-EXAFS data showed the increase of the Pd−Pd contribution (light green area in Figure 3b) which evidenced that the Pd(0) species formed in the microchip are represented by palladium nanoparticles. Due to the small size of the particles, the intensity of the Pd−Pd contribution in FT-EXAFS data (which is proportional to the average coordination number) is significantly lower in comparison with bulk palladium.

Linear combination fitting was used to quantify the amount of Pd(0) and Pd(II) species in each channel (Figure 4a). In the

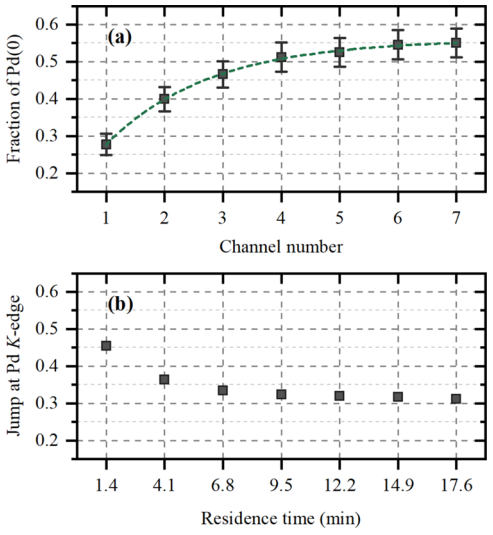

Figure 4. (a) Evolution of Pd(0) fraction (black squares) over the first seven channels of the microchip obtained by fitting the experimental XANES data by the reference spectra of palladium(II) acetate and palladium foil. The green dashed line corresponds to the exponential fit of the data. (b) Changes in the edge jump in XAS data, which is proportional to the total concentration of palladium in the channel.

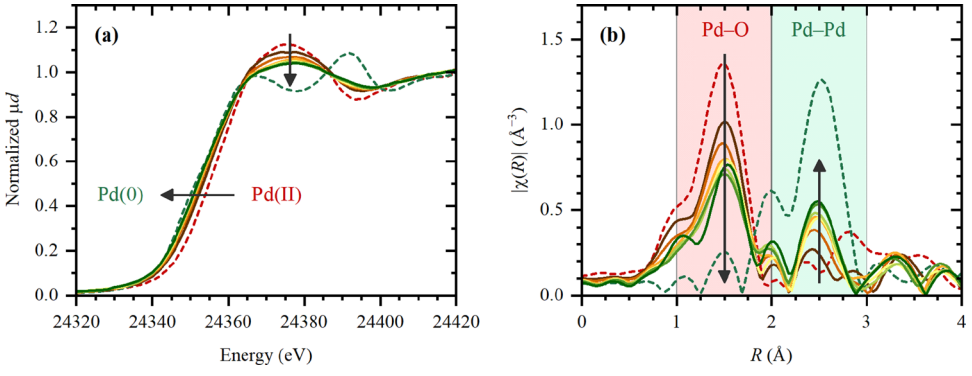

Figure 3. Evolution of XANES (a) and FT-EXAFS (b) data collected in situ in different channels of the microchip (solid lines, from brown to green). Dashed red and green lines correspond to the reference palladium(II) acetate and palladium foil, respectively. The FT-EXAFS spectrum of Pd foil in part (b) is scaled by 0.5 for visualization purposes.

https://doi.org/10.1021/acs.jpcc.3c03266
J. Phys. Chem. C XXXX, XXX, XXX−XXX

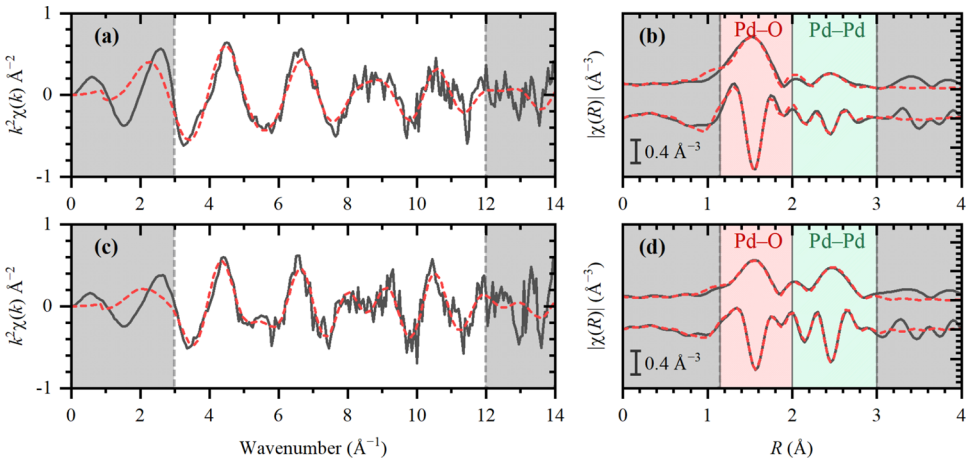

Figure 5. Experimental (solid black) and fitted (dashed red) EXAFS data in *k*-space (a, c) and magnitudes and imaginary parts in *R*-space (b, d) for channels #1 (a, b) and #7 (c, d). The gray background shows the regions excluded from the fit.

Table 2. Interatomic Distances (R), Coordination Numbers (N), Debye–Waller Parameters (σ^2), Zero Energy Shift (ΔE_0), and the Relative Fractions (α) for the Pd–O and Pd–Pd Contribution Obtained from EXAFS Analysis for the Data Collected at Channel #7

path	R (Å)	N	σ^2	ΔE_0	α
Pd–O	2.01 ± 0.01	4[a]	0.001 ± 0.001	2.9 ± 0.8	0.41 ± 0.04
Pd–Pd	2.75 ± 0.02	3.6 ± 0.5	0.006 ± 0.001	−3.0 ± 0.8	0.59[b]

[a]Fixed. [b]Fixed to $1 - \alpha_{Pd-Pd}$.

seventh channel, the Pd(0) concentration is close to the saturated value of 0.56 obtained by fitting the Pd(0) concentrations by an exponential function (green dashed line in Figure 4a). However, the actual amount of Pd(0) particles obtained by such method may be significantly underestimated since the actual state of small palladium nanoparticles is expected to have a strong contribution from the interaction of surface atoms with the solvent and capping agent and can differ from palladium foil used as a reference of linear combination fitting. Notably, despite the difference in the spectral shape, the position of the absorption edge, which is indicative of the oxidation state, is very close to that of palladium foil. The change in the absolute value of the edge jump, which is proportional to the total concentration of palladium in each channel, was also investigated. A decrease of ca. 32% from the first to seventh channel was observed (Figure 4b) which was associated with the precipitation of the particles on the walls of the microchannels. The Pd concentration calculated based on the edge jump is decreasing from 7.5 to 5.5 μmol/mL. Given the volume of the cell and the speed of the flow, the residence time was also calculated (the abscissa axis in Figure 4b).

Quantitative EXAFS analysis (Figure 5 and Table 2) further proved the formation of Pd–Pd bonds of 2.75 ± 0.02 Å, as in metallic palladium foil. At the same time, a strong signal of Pd–X (X = C, N, O, which are indistinguishable by EXAFS) is present at 2.01 ± 0.01 Å. To extract the particle size based on the average Pd–Pd coordination numbers, the following model was applied. The Pd–X (Pd–O) coordination number was fixed to 4 as in the palladium precursor and the Pd–O contribution was multiplied by $S_0^2 \cdot 4 \cdot \alpha$, where α is the remaining fraction of Pd precursor and S_0^2 is the amplitude reduction factor fixed to 0.8 as determined for the reference palladium foil. The Pd–Pd contribution was multiplied by $S_0^2 \cdot N_{Pd-Pd} \cdot (1 - \alpha)$, where N_{Pd-Pd} is the average coordination number. The obtained N_{Pd-Pd} of 3.6 corresponds to the particle size of 0.5 nm in an assumption of ideal spherical particles with *fcc* structure (with the first shell coordination number of 12):

$$N_{Pd-Pd} = 12\left[1 - \frac{3}{2}\frac{R_{Pd-Pd}}{D} + \frac{1}{2}\left(\frac{R_{Pd-Pd}}{D}\right)^3\right] \quad (1)$$

where R_{Pd-Pd} is the first shell Pd–Pd distance and D is the mean particle size.

However, if the particles have defects or deviate from the *fcc* lattice, such determination will underestimate the real particle size.

DISCUSSION

The suggested methodology allowed for in situ XAS data collection of high quality for a low-concentrated system during the formation of palladium nanoparticles in solution. In particular, the edge jump of almost 0.5 was obtained, which is only twice lower than the optimal one, normally obtained for ex situ (solid) samples. This allowed us to utilize EXAFS data up to $k \sim 12$ Å^{-1} for the spectra collected in situ, with the time acquisition of only 10 min at the second-generation synchrotron source. The quality of the signal in *k*-space can be easily appreciated from Figure 5a, which is crucial for EXAFS analysis. For comparison, in other in situ cells (see, e.g., ref 21), a similar quality of the data was achieved for much higher concentrated systems using a significantly more advanced synchrotron source (and ca. 5 orders of magnitude higher photon flux).

It should also be noted that the Pd–Pd interatomic obtained for the formed palladium clusters is similar to that of the bulk palladium foil. Although a contraction of metal–metal distances can be expected for palladium nanoparticles, this result is in agreement with our previous studies of supported Pd particles with sizes from 1 to 10 nm on various

https://doi.org/10.1021/acs.jpcc.3c03266
J. Phys. Chem. C XXXX, XXX, XXX–XXX

supports.[22−28] The elongation of Pd−Pd distances can be caused by the presence of H or C atoms easily forming palladium hydrides[29,30] and carbides[31−33] and expanding the lattice. A similar explanation was presented by Ciapina and co-workers who concluded that H or C atoms can originate from catalytic decomposition of the organic compounds present during the synthesis.[34]

At the same time, the total volume of the sample used during the experiment was around a few milliliters, and the total amount of Pd precursor spent for the whole experiment was less than 20 mg (in comparison, this is even less than one needs for a pellet of 13 mm for standard ex situ XAS measurement of Pd(II) acetate). It should also be noted that due to the low price and well-developed technology of 3D printing, such microchips can be easily tuned and optimized for any particular liquid system depending on the total absorption of the solvent itself, concentration of metal, etc. In addition, it should be noted that such geometry is advantageous with respect to perpendicular one with the measurement of XAS in fluorescence mode, which is also because in the latter case, the X-ray beam can induce additional processes (e.g., photoreduction, nucleation, and radiation damage) on the chip/liquid interface which will significantly contribute to the collected XAS signal, whereas in the presented geometry, even if this would be the case, its contribution to the total spectrum averaged over the whole channel is negligible. Finally, the fact that the growth of Pd clusters is observed over all seven channels while the decrease of Pd concentration is negligible starting already from the second channel (Figure 4b) suggests that the observed evolution is not affected (at least significantly) by the beam damage effects.

The elements with absorption edges in the hard X-ray range, such as Pd, are obviously advantageous systems for such experiments since the absorption by the organic solvent at these energies is very low. For *K*-edges of 3*d* metals and *L*-edges of 5*d* metals, the optimization of the microchannel length will be strongly limited by the absorption of the solvent. Even for high energies, the solvent should also be taken into account and chosen carefully. For example, the DMSO at Pd *K*-edge absorbs about 6 times stronger than water and about 20 times stronger than toluene. Additional synchronization of X-ray data collection in transmission mode, in contrast to fluorescence where this is less an issue, with the flow rate should be made in the case of using a segmented flow.

Finally, it should be noted that the good quality of the EXAFS spectrum is achieved at the expense of the time resolution which is reduced due to the averaging of the signal over the length of the channel. On the one hand, this problem can be solved by increasing the reactant flow or reducing the thickness of the microchannels. For example, reducing the channel diameter below 1 mm as in most of the current microfluidic devices will still be sufficient for XAS measurement at modern synchrotron beamlines whose optics can provide beam focusing down to the 100 μm range. However, it has to be considered that both flow rate and channel geometry can affect the reaction by changing the mixing pattern. On the other hand, the photon flux at most of the modern EXAFS beamlines is 3−5 orders of magnitude higher than that used in the current work, which will allow obtaining high-quality data from much shorter channels, improving the time resolution (e.g., reducing the channel length to 10 mm would still give a reasonable edge jump of ca. 0.05).

CONCLUSIONS

We have successfully demonstrated the strategy for in situ XAS monitoring of the chemical process inside the microfluidic devices with exceptional data quality due to the collection of spectra in transmission geometry by aligning the microchannels along the direction of the X-ray beam. A gradual reduction of Pd(II) acetate with the formation of small Pd(0) particles was observed by probing different microchannels. As most of the previous reports on coupling XAS with microfluidics,[12−16] this work is methodological, but the suggested strategy can be definitely used to gain important chemical insights for a wide range of processes involving the elements with the absorption edges in the hard X-ray range, especially 4*d* metals.

AUTHOR INFORMATION

Corresponding Author

Aram L. Bugaev − *Paul Scherrer Institute, 5232 Villigen, Switzerland;* orcid.org/0000-0001-8273-2560; Email: aram.bugaev@psi.ch

Authors

Arina V. Dobrovolskaya − *The Smart Materials Research Institute, Southern Federal University, 344090 Rostov-on-Don, Russia*

Sergei V. Chapek − *The Smart Materials Research Institute, Southern Federal University, 344090 Rostov-on-Don, Russia*

Oleg A. Usoltsev − *The Smart Materials Research Institute, Southern Federal University, 344090 Rostov-on-Don, Russia;* orcid.org/0000-0002-1537-3497

Evgeny Naranov − *Topchiev Institute of Petrochemical Synthesis, Russian Academy of Sciences, 119991 Moscow, Russia;* orcid.org/0000-0002-3815-9565

Dmitry N. Gorbunov − *Topchiev Institute of Petrochemical Synthesis, Russian Academy of Sciences, 119991 Moscow, Russia;* orcid.org/0000-0002-1603-8957

Alexander L. Trigub − *National Research Centre "Kurchatov Institute", 123182 Moscow, Russia*

Anton L. Maximov − *Topchiev Institute of Petrochemical Synthesis, Russian Academy of Sciences, 119991 Moscow, Russia*

Alexander V. Soldatov − *The Smart Materials Research Institute, Southern Federal University, 344090 Rostov-on-Don, Russia*

Complete contact information is available at: https://pubs.acs.org/10.1021/acs.jpcc.3c03266

Notes

The authors declare no competing financial interest.

ACKNOWLEDGMENTS

The authors acknowledge the Ministry of Science and Higher Education of the Russian Federation for financial support of synchrotron measurements (Agreement No 075-15-2021-1363). The development of synthetic protocol and microfluidic chip was supported by the Strategic Academic Leadership Program of the Southern Federal University ("Priority 2030").

REFERENCES

(1) Convery, N.; Gadegaard, N. 30 years of microfluidics. *Micro Nano Eng.* **2019**, *2*, 76−91.

(2) Marre, S.; Jensen, K. F. Synthesis of micro and nanostructures in microfluidic systems. *Chem. Soc. Rev.* **2010**, *39*, 1183−1202.
(3) Luo, G.; Du, L.; Wang, Y.; Lu, Y.; Xu, J. Controllable preparation of particles with microfluidics. *Particuology* **2011**, *9*, 545−558.
(4) Song, Y.; Hormes, J.; Kumar, C. S. S. R. Microfluidic synthesis of nanomaterials. *Small* **2008**, *4*, 698−711.
(5) Solsona, M.; Vollenbroek, J. C.; Tregouet, C. B. M.; Nieuwelink, A. E.; Olthuis, W.; van den Berg, A.; Weckhuysen, B. M.; Odijk, M. Microfluidics and catalyst particles. *Lab Chip* **2019**, *19*, 3575−3601.
(6) Pena-Pereira, F.; Costas-Mora, I.; Romero, V.; Lavilla, I.; Bendicho, C. Advances in miniaturized UV-Vis spectrometric systems. *TrAC Trends Anal. Chem.* **2011**, *30*, 1637−1648.
(7) Chrimes, A. F.; Khoshmanesh, K.; Stoddart, P. R.; Mitchell, A.; Kalantar-Zadeh, K. Microfluidics and Raman microscopy: current applications and future challenges. *Chem. Soc. Rev.* **2013**, *42*, 5880−5906.
(8) Chen, X.; Wang, J.; Pan, R.; Roth, S.; Förster, S. Insights into growth kinetics of colloidal gold nanoparticles: In Situ SAXS and UV−Vis evaluation. *J. Phys. Chem. C* **2021**, *125*, 1087−1095.
(9) Ilhan-Ayisigi, E.; Yaldiz, B.; Bor, G.; Yaghmur, A.; Yesil-Celiktas, O. Advances in microfluidic synthesis and coupling with synchrotron SAXS for continuous production and real-time structural characterization of nano-self-assemblies. *Colloids Surf., B Biointerfaces* **2021**, *201*, No. 111633.
(10) Beuvier, T.; Panduro, E. A.; Kwasniewski, P.; Marre, S.; Lecoutre, C.; Garrabos, Y.; Aymonier, C.; Calvignac, B.; Gibaud, A. Implementation of in situ SAXS/WAXS characterization into silicon/glass microreactors. *Lab Chip* **2015**, *15*, 2002−2008.
(11) Levenstein, M. A.; Anduix-Canto, C.; Kim, Y.-Y.; Holden, M. A.; González Niño, C.; Green, D. C.; Foster, S. E.; Kulak, A. N.; Govada, L.; Chayen, N. E.; et al. Droplet microfluidics XRD identifies effective nucleating agents for calcium carbonate. *Adv. Funct. Mater.* **2019**, *29*, No. 1808172.
(12) Chaussavoine, I.; Beauvois, A.; Mateo, T.; Vasireddi, R.; Douri, N.; Priam, J.; Liatimi, Y.; Lefrancois, S.; Tabuteau, H.; Davranche, M.; et al. The microfluidic laboratory at Synchrotron SOLEIL. *J. Synchrotron Radiat.* **2020**, *27*, 230−237.
(13) Micheal Raj, P.; Barbe, L.; Andersson, M.; De Albuquerque Moreira, M.; Haase, D.; Wootton, J.; Nehzati, S.; Terry, A. E.; Friel, R. J.; Tenje, M.; et al. Fabrication and characterisation of a silicon-borosilicate glass microfluidic device for synchrotron-based hard X-ray spectroscopy studies. *RSC Adv.* **2021**, *11*, 29859−29869.
(14) Hofmann, G.; Tofighi, G.; Rinke, G.; Baier, S.; Ewinger, A.; Urban, A.; Wenka, A.; Heideker, S.; Jahn, A.; Dittmeyer, R.; Grunwaldt, J. D. A microfluidic device for the investigation of rapid gold nanoparticle formation in continuous turbulent flow. *J. Phys. Conf. Ser.* **2016**, *712*, No. 012072.
(15) Oyanagi, H.; Sun, Z. H.; Jiang, Y.; Uehara, M.; Nakamura, H.; Yamashita, K.; Zhang, L.; Lee, C.; Fukano, A.; Maeda, H. In situ XAFS experiments using a microfluidic cell: application to initial growth of CdSe nanocrystals. *J. Synchrotron Radiat.* **2011**, *18*, 272−279.
(16) Probst, J.; Borca, C. N.; Newton, M. A.; van Bokhoven, J.; Huthwelker, T.; Stavrakis, S.; deMello, A. In situ X-ray absorption spectroscopy and droplet-based microfluidics: An analysis of calcium carbonate precipitation. *ACS Meas. Sci. Au* **2021**, *1*, 27−34.
(17) Janssens, K.; Bugaev, A. L.; Kozyr, E. G.; Lemmens, V.; Guda, A. A.; Usoltsev, O. A.; Smolders, S.; Soldatov, A. V.; De Vos, D. E. Evolution of the active species of homogeneous Ru hydrodeoxygenation catalysts in ionic liquids. *Chem. Sci.* **2022**, *13*, 10251−10259.
(18) Shvets, P. V.; Prokopovich, P. A.; Dolgoborodov, A. I.; Usoltsev, O. A.; Skorynina, A. A.; Kozyr, E. G.; Shapovalov, V. V.; Guda, A. A.; Bugaev, A. L.; Naranov, E. R.; et al. In situ X-ray absorption spectroscopy cells for high pressure homogeneous catalysis. *Catalysts* **2022**, *12*, 1264.
(19) Pandit, L.; Serrer, M. A.; Saraçi, E.; Boubnov, A.; Grunwaldt, J. D. Versatile in situ/operando setup for studying catalysts by X-ray absorption spectroscopy under demanding and dynamic reaction conditions for energy storage and conversion. *Chem. Methods* **2022**, *2*, No. e202100078.
(20) Ravel, B.; Newville, M. ATHENA, ARTEMIS, HEPHAESTUS: data analysis for X-ray absorption spectroscopy using IFEFFIT. *J. Synchrotron Radiat.* **2005**, *12*, 537−541.
(21) Yuan, N.; Pascanu, V.; Huang, Z.; Valiente, A.; Heidenreich, N.; Leubner, S.; Inge, A. K.; Gaar, J.; Stock, N.; Persson, I.; et al. Probing the evolution of palladium species in Pd@MOF catalysts during the heck coupling reaction: An operando X-ray absorption spectroscopy study. *J. Am. Chem. Soc.* **2018**, *140*, 8206−8217.
(22) Bugaev, A. L.; Skorynina, A. A.; Braglia, L.; Lomachenko, K. A.; Guda, A.; Lazzarini, A.; Bordiga, S.; Olsbye, U.; Lillerud, K. P.; Soldatov, A. V.; et al. Evolution of Pt and Pd species in functionalized UiO-67 metal-organic frameworks. *Catal. Today* **2019**, *336*, 33−39.
(23) Kamyshova, E. G.; Skorynina, A. A.; Bugaev, A. L.; Lamberti, C.; Soldatov, A. V. Formation and growth of Pd nanoparticles in UiO-67 MOF by in situ EXAFS. *Radiat. Phys. Chem.* **2020**, *175*, No. 108144.
(24) Bugaev, A. L.; Zabilskiy, M.; Skorynina, A. A.; Usoltsev, O. A.; Soldatov, A. V.; van Bokhoven, J. A. In situ formation of surface and bulk oxides in small palladium nanoparticles. *Chem. Commun.* **2020**, *56*, 13097−13100.
(25) Bugaev, A. L.; Guda, A. A.; Lomachenko, K. A.; Srabionyan, V. V.; Bugaev, L. A.; Soldatov, A. V.; Lamberti, C.; Dmitriev, V. P.; van Bokhoven, J. A. Temperature- and pressure-dependent hydrogen concentration in supported PdH_x nanoparticles by Pd K-edge X-ray absorption spectroscopy. *J. Phys. Chem. C* **2014**, *118*, 10416−10423.
(26) Srabionyan, V. V.; Bugaev, A. L.; Pryadchenko, V. V.; Avakyan, L. A.; van Bokhoven, J. A.; Bugaev, L. A. EXAFS study of size dependence of atomic structure in palladium nanoparticles. *J. Phys. Chem. Solids* **2014**, *75*, 470−476.
(27) Van Velthoven, N.; Henrion, M.; Dallenes, J.; Krajnc, A.; Bugaev, A. L.; Liu, P.; Bals, S.; Soldatov, A. V.; Mali, G.; De Vos, D. E. S,O-Functionalized metal-organic frameworks as heterogeneous single-site catalysts for the oxidative alkenylation of arenes via C-H activation. *ACS Catal.* **2020**, *10*, 5077−5085.
(28) Usoltsev, O. A.; Skorynina, A. A.; Protsenko, B. O.; Martin-Diaconescu, V.; Pellegrini, R.; Soldatov, A. V.; van Bokhoven, J.; Bugaev, A. L. Evolution of surface and bulk structure of supported palladium nanoparticles by in situ X-ray absorption and infrared spectroscopies: Effect of temperature, CO and CH_4 gas. *Appl. Surf. Sci.* **2023**, *614*, No. 156171.
(29) Bugaev, A. L.; Guda, A. A.; Lomachenko, K. A.; Lazzarini, A.; Srabionyan, V. V.; Vitillo, J. G.; Piovano, A.; Groppo, E.; Bugaev, L. A.; Soldatov, A. V.; Dmitriev, V. P.; Pellegrini, R.; van Bokhoven, J. A.; Lamberti, C. Hydride phase formation in carbon supported palladium hydride nanoparticles by in situ EXAFS and XRD. *J. Phys. Conf. Ser.* **2016**, *712*, No. 012032.
(30) Bugaev, A. L.; Srabionyan, V. V.; Soldatov, A. V.; Bugaev, L. A.; van Bokhoven, J. A. The role of hydrogen in formation of Pd XANES in Pd-nanoparticles. *J. Phys. Conf. Ser.* **2013**, *430*, No. 012028.
(31) Bugaev, A. L.; Guda, A. A.; Pankin, I. A.; Groppo, E.; Pellegrini, R.; Longo, A.; Soldatov, A. V.; Lamberti, C. The role of palladium carbides in the catalytic hydrogenation of ethylene over supported palladium nanoparticles. *Catal. Today* **2019**, *336*, 40−44.
(32) Skorynina, A. A.; Tereshchenko, A. A.; Usoltsev, O. A.; Bugaev, A. L.; Lomachenko, K. A.; Guda, A. A.; Groppo, E.; Pellegrini, R.; Lamberti, C.; Soldatov, A. V. Time-dependent carbide phase formation in palladium nanoparticles. *Radiat. Phys. Chem.* **2020**, *175*, 108079.
(33) Bugaev, A. L.; Guda, A. A.; Lazzarini, A.; Lomachenko, K. A.; Groppo, E.; Pellegrini, R.; Piovano, A.; Emerich, H.; Soldatov, A. V.; Bugaev, L. A.; et al. In situ formation of hydrides and carbides in palladium catalyst: when XANES is better than EXAFS and XRD. *Catal. Today* **2017**, *283*, 119−126.
(34) Ciapina, E. G.; dos Santos, M. L.; Santos, R. M. I. S.; Palombarini, J.; Almeida Júnior, O. P.; Santana, J. C. C. d. C.; Modesto, D. A.; Lanfredi, A. J. C.; Santos, S. F. On the lattice dilation

https://doi.org/10.1021/acs.jpcc.3c03266
J. Phys. Chem. C XXXX, XXX, XXX−XXX

of palladium nanoparticles and a new methodology for the quantification of interstitials. *J. Alloys Compd.* **2021**, *881*, No. 160628.

https://doi.org/10.1021/acs.jpcc.3c03266
J. Phys. Chem. C XXXX, XXX, XXX−XXX